

Animation of Soap Bubble Dynamics, Cluster Formation and Collision

Roman Ďurikovič[†],

Computer Graphics Laboratory, Software Department, The University of Aizu,
Ikki-machi, Aizuwakamatsu-shi, Fukushima, 965 8580 Japan.
email: roman@u-aizu.ac.jp

Abstract

What is happening when a soap bubble floats on the air? How do bubbles coalesce to form beautiful three-dimensional clusters? The physical-based model and animation described herein provide the answers. This paper deals with a complete computer simulation of soap bubbles from a dynamic perspective, which should prove to be of great interest to physicists and mathematicians. We discuss the dynamic formation of irregular bubble clusters and how to animate bubbles. The resulting model takes into account surface tension, film elasticity, and shape variations due to gravity and external wind forces.

1. Introduction

Foams are of great interest to physicists and chemists studying macroscopic and molecular surface properties such as wetting, dyeing, foaming, coalescing and emulsification. Mathematicians have long been concerned with problems that require minimization of surface areas contained by a fixed boundary. Euler has investigated variational methods to prove the existence of geometric properties associated with minimum-area surfaces and to solve minimum-area problems. Finding the minimal surface of a boundary with specified constraints, usually having no surface singularities, is known as Plateau's problem in calculus of variations. Generally, there may be one, multiple, or no minimal surface spanning on a given closed curve in space. Despite substantial efforts made to obtain an analytic solution, only in the 1930s was the existence of a solution for the general case proven by Douglas[?] and Rado[?], although their analysis could not exclude the possibility of singularities. Plateau showed that the solution to some special cases could be produced by dipping wire frameworks into a bath of soap solution.

Some experiments, however, are not possible without resorting to numerical calculation. Although the lifetime of

pure soap bubbles can be prolonged by special bubble solutions containing glycerine, the bubbles are sensitive to the presence of impurities, dust particles, excess of caustic alkali or fat, making their study difficult. It is therefore necessary to create a plausible dynamic model capable of three-dimensional bubble clustering simulation.

There have been recent studies of interference produced by thin films[?] including effective summaries of thin-film geometries. More advanced methods take into account thickness variation of bubble films under gravity and derive equations describing the interaction between a plane monochromatic electromagnetic wave and the film[?]. The bubble clusters in such studies are considered to be the union of spherical shells and spherical caps calculated mostly with set theoretic operations usually implemented in ray-tracing algorithms.

The aim of this study is to suggest a dynamic, physically based model of a soap bubble that can simulate bubble formation, deformation, collision with a planar surface, and dynamic collision of two bubbles. Section 2 recalls the attainments on the geometrical arrangements of a collection of bubbles of different sizes, in particular double-bubble and triple-bubble configurations. Predominant surface tension involved in bubble dynamics is described in Section 3, and here we propose an interval range based on statistical deviations of surface tension for different soap solution concentrations. The measured values are then used in a proposed

[†] On leave from Department of Computer Graphics and Image Processing, Faculty of Mathematics and Physics, Comenius University, 820 13 Bratislava, Slovakia.

dynamic model of a single bubble in Section 4. In Section 5, we derive the dynamics of bubble collision with a plane and apply it to double-bubble coalescence. The final section, which is followed by conclusions, presents animated frames of simulated bubble formation, deformation and clustering.

2. Soap Film Configurations

A bubble is the minimal energy surface of a type formed by a soap film. In relation to its volume, it has the smallest surface.

2.1. Plateau's Laws

Analog solutions to the minimization problems can be produced by dipping wire frames into a soap-solution bath, as shown by experimentalist Plateau². The minimum surface thus produced was found to have common geometrical properties for multiple bubbles, and can be stated as:

1. Three smooth surfaces of a soap film intersect along a line.
2. The angle between any two tangent planes to the intersecting surfaces, at any point along the line of intersection of three surfaces, is 120° .
3. Only four edges can join at a vertex, each formed by the intersection of three surfaces, forming together the tetrahedral angle $109^\circ 28' 16''$ between any pair of adjacent lines.

Soap froth consists of a collection of bubbles of different sizes, with shape and arrangement governed by the first two of Plateau's rules. When a cluster is formed from bubbles of different radii the internal surfaces are curved due to pressure differences, as stated in Section 2.2. The third rule applies only to minimal surfaces formed by a frame and not to soap froth.

2.2. Double Bubble

A double bubble is a pair of bubbles that intersect and are separated by a membrane bounded by the intersection. The double bubble illustrated in Figures 1 and 2 can have two possible configurations: an ordinary configuration in which two spherical shells are connected, and a nonstandard configuration in which one bubble is toroidal and the other dumbbell shaped. It had been conjectured that two equal partial spheres sharing a boundary of a flat disk separate two separate volumes of air using a total surface area that is less than any other boundary. This case of two bubbles having the same size was proved by J. Hass and R. Schlafy, who reduced the problem to a set of 200 260 integrals. Finally, M. Hutchings *et al.* proved the conjecture for arbitrary double bubbles in R^{n+1} , in March 2000³. They showed that there is no nonstandard double bubble stable in R^{n+1} , which explains why we do not observe such configurations in nature.

The double bubble is thus area minimizing. It is not known, however, whether the triple bubble is also minimizing. Also unknown is whether empty chambers trapped inside the cluster can minimize area for the number of bubbles $n \geq 3$.

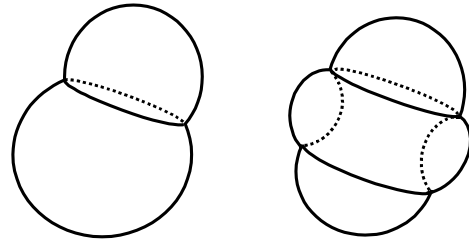


Figure 1: Double bubble configurations. left: standard and right: nonstandard.

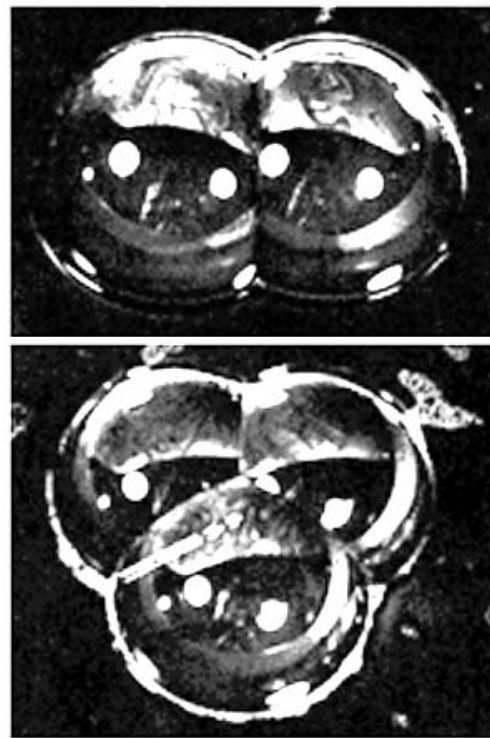


Figure 2: Photographs of real double bubble and triple bubble configurations.

2.2.1. Geometry

The major part of each bubble in a double-bubble configuration consists of spherical shells of soap film separated by a spherical cap of soap film. If the bubbles are of different size, the smaller bubble, which always has a higher internal

pressure, will intrude into the larger bubble. Figure 3 shows the configuration of two bubbles with radii r_A and r_B and internal pressures P_A and P_B resulting from Plateau's laws. It is possible to show that the general property concerning the intersection of three surfaces of soap film at angles 120° provides a method for obtaining the following reciprocal relation ^{2,3}

$$\frac{1}{r_B} = \frac{1}{r_A} + \frac{1}{r_C}, \quad (1)$$

where r_C is the radius of the common surface. Let M be an arbitrary point where the three surfaces of soap film meet. The cosine rule for the triangle AMB states that $AB^2 = r_A^2 + r_B^2 + 2r_A r_B \cos(\angle AMB)$, where the angle $\angle AMB = 60^\circ$. The distance between bubble centers A to B , therefore, can be derived as

$$AB^2 = r_A^2 + r_B^2 - r_A r_B. \quad (2)$$

Considering the triangle AMC and angle $\angle AMC = 120^\circ$, an equivalent equation can be derived for the distance AC , e.g.

$$AC^2 = r_A^2 + r_C^2 + r_A r_C.$$

The excess pressure across the surface common to regions A and B , p_{AB} , given by the Laplace-Young equation is constant and related to the radius of the partitioning surface by

$$p_{AB} = P_A - P_B = \frac{4\gamma}{r_C}, \quad (3)$$

where γ is the surface tension of a liquid mixture.

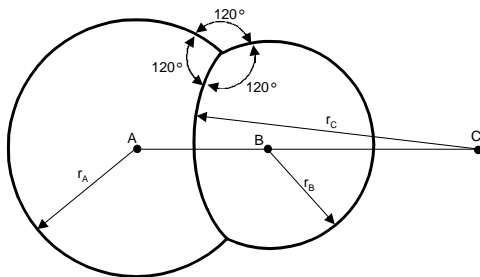


Figure 3: Curvatures of double bubble shells.

2.3. Triple Bubble

When three bubbles are in contact with one another, as shown in Figure 4, three interfaces meet, as well as three spherical shells all at angles of 120° . The centers of curvature of the three bubbles A, B, D and of the three interfaces necessarily lie in a single plane. The centers of curvature of the three interfaces lie in a straight line, marked by C, E , and F .

Looking at a triple-bubble configuration as three double-bubble compositions, one realizes that the relationship in

Eq. 1 holds for each pair of bubbles, and thus there are two additional reciprocal relationships

$$\frac{1}{r_D} = \frac{1}{r_A} + \frac{1}{r_E}, \quad \frac{1}{r_D} = \frac{1}{r_B} + \frac{1}{r_F},$$

where the radius of the third bubble is r_D . Two separating surfaces are newly created with radiuses r_E and r_F between the bubbles with centers A, D , and between the bubbles with centers B, D , respectively. Analogically to Eq. 2, the distances between bubble centers A to D and B to D will be

$$AD^2 = r_A^2 + r_D^2 - r_A r_D, \quad BD^2 = r_B^2 + r_D^2 - r_B r_D.$$

Finally, the excess pressure across the surfaces common to regions A, D , and B, D is given by following equations:

$$p_{AD} = P_A - P_D = \frac{4\gamma}{r_E}, \quad p_{BD} = P_B - P_D = \frac{4\gamma}{r_F}.$$

The above statements, unfortunately, have not been proven to minimize the surface area. Nevertheless, they are generally used in calculations of thin film arrangements because their implications from Plateau's laws have been supported in numerous experiments.

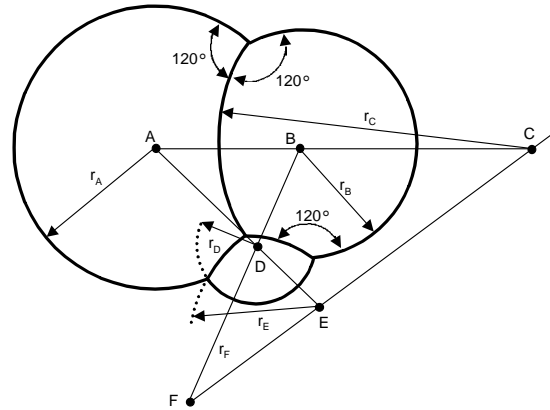


Figure 4: Curvatures of triple bubble shells.

2.4. N-bubble

One outstanding problem involving bubbles is the determination of the bubble arrangements with the smallest surface areas enclosing and separating n given volumes in space. The cluster of bubbles illustrates Plateau's three laws, fortunately, and thus the statements derived for a triple bubble also hold for each triple bubble in foam.

The Laplace-Young equation used in its simple form in Eqs. 1 and 3 resulted from zero excess pressure across any point on the surface of the soap film, which is not true for general bubble clusters. The Laplace-Young equation, however, can be applied in these general conditions and Equations 1, and 3 can also be generalized to foams.

Bubbles can produce hemispherical clusters when formed on a wet planar surface or on the surface of a soap-solution bath. The angles of intersecting surfaces are equal to 120° , while the angle between the bubble hemisphere and the planar surface is 90° .

3. Surface Tension

Within the water, at least a few molecules away from the surface, each molecule is connected with its neighbors on every side, so that any given molecule feels no net force. At the surface, however, things are different. There is no upward pull for every downward pull, since of course there is no liquid above the surface. Thus the surface molecules tend to be pulled back into the liquid. If the surface is stretched - as when you blow up a bubble - it becomes larger in area, and more molecules are dragged from within the liquid to become part of this increased area. This "stretchy skin" effect is called surface tension. Surface tension plays an important role in the way liquids behave.

3.1. Soap Solution

In a soap-and-water solution, the hydrophobic (greasy) ends of the soap molecule resist being in the liquid at all. Those that find their way to the surface squeeze between the surface water molecules, pushing their hydrophobic ends out of the water. This separates the water molecules from each other, decreasing the attractive force between them. Since the surface tension forces become smaller as the distance between water molecules increases, the intervening soap molecules decrease the surface tension.

3.2. Measurement

The rise of a liquid in a capillary tube is still the standard laboratory technique for the precise measurement and comparison of surface tensions. We have measured the viscosity of several bubble solutions discovered by bubble artists at a constant temperature of 20°C . At part of the surface, the gravity of liquid in the tube and the surface tension against air are equal (see Figure 5). Thus, the surface tension of the liquid with density ρ_2 against the surrounding gas ρ_1 can be derived from the Laplace-Young equation as follows:

$$\gamma = \frac{\Delta\rho r(h - \Delta h)}{2 \cos \theta},$$

where $\Delta\rho = \rho_2 - \rho_1$ is the density difference, r is the tube radius, g is the gravitational acceleration, h is the height of the liquid column, and Δh is the height of the meniscus lens of liquid above h . In the case of pure water, θ is nearly equal to 0 at 20°C and it has the surface tension $\gamma_w = 0.072\text{N/m}$. The surface tension of a bubble solution against air was found to be about one third that of water, and varies with the concentration of soap solution. Therefore, the interval range derived from statistical deviations is proposed to be $\gamma_s \in (0.0195, 0.0265)$.

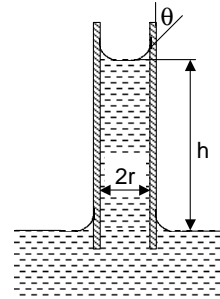


Figure 5: The rise of liquid in capillary tube.

4. Dynamics

Direct experiments summarized by Boys² have shown that a soap film, or bubble, is elastic. One can notice at least two things: large bubbles recover their shape slowly, while small bubbles become round much more quickly. Eventually, a large bubble oscillates much more slowly than a small one when it is knocked out of shape. Different kinds of energies are involved: potential energy, energies of interaction between film surfaces, and surface tension.

In this research we engaged in constraint-based modeling of deformable models. In actual practice, we will consider the elastic model developed in Terzopoulos and Fleischer². The equation of motion governing the elastic deformable model is:

$$M \frac{\partial^2 x_i}{\partial t^2} = F_i(t) - \gamma \frac{\partial x_i}{\partial t} - \frac{\delta \epsilon(x)}{\delta x_i}, \quad (4)$$

where x_i is the position of mass particle i of the object, M is the mass density, γ is the damping constant, $F_i(t)$ is the net externally applied force, and $\delta \epsilon(x)/\delta x$ is the internal energy that resists deformation. After discretizing the equation, it can be rewritten as a set of first-order differential equations in the canonical form.

5. Applied Forces

The geometrical model of a bubble used in simulation is constructed of masses and springs governed by Lagrange's equation of motion, Eq. 4. The initial state of the bubble's geometrical model is a sphere subdivided into equilateral triangles, with the corners representing the particles and edges corresponding to damped springs. The force from the springs corresponds to the total internal force $\delta \epsilon(x)/\delta x$ in the equation of motion. This section discusses all external forces comprising gravity, excess pressure, external fluid, repulsive, and interaction forces

$$F_i(t) = F_{grav} + F_{excess} + F_{drag} + F_{rep} + F_{lennard} + F_{plane} + \dots$$

The total force acting on a particle, illustrated in Figure 6, determines the accelerations from which velocities and new positions can be extrapolated by integrating Eq. 4.

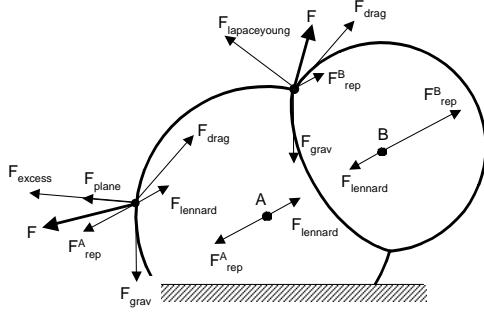


Figure 6: External forces applied on a particle. The excess pressure force, F_{excess} , is applied on particles belonging to spherical shells while Laplace-Young force, $F_{laplaceyoung}$, is used for other particles.

5.1. Gravity

The gravity is an external force acting on particle i , $F_{grav} = m_i g$. The mass of a single particle is derived from the density ρ and total volume V of soap liquid $m_i = \rho V/n$, where n is the number of particles.

5.2. Excess Pressure Force

The direction of the pressure force at any one point is heading in the direction of the surface normal vector at that point. Similar to Eq. 3, the excess pressure between the interior of spherical bubble P_A and that of outer space P_O is known to be $P_{AO} = P_A - P_O = \frac{4\gamma_s}{r_A}$, where γ_s is the surface tension for the liquid-air interface and r_A is the radius of bubble. Therefore, we can propose the force due to the excess pressure acting on a given particle i

$$F_{excess}^i = 4w_0 \frac{\gamma_s}{R_i} A_i N_i, \quad (5)$$

where R_i is a local radius of mean curvature at particle i , the total area of adjusted triangles is A_i , N_i is the unit normal vector, and w_0 is the unit conversion constant. The local radius of curvature can be estimated as follows:

$$R_i = \frac{1}{K_i^{\frac{1}{2}}},$$

$$K_i = (3\Delta\theta)/A_i, \quad \Delta\theta = 2\pi - \sum \theta_j,$$

$$\theta_j = \arccos\left[\frac{l_j^2 + l_{j+1}^2 - p_j^2}{2l_j l_{j+1}}\right], \quad A_i = \sum a_j,$$

$$a_j = [s(s-l_j)(s-l_{j+1})(s-p_j)]^{\frac{1}{2}},$$

where $s = (l_j + l_{j+1} + p_j)/2$, see Figure 7. Note that all elements of excess pressure force are derived based on the geometric information only.

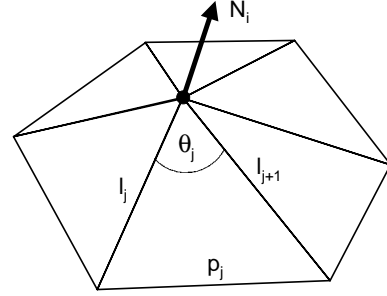


Figure 7: Curvature estimation.

5.3. Laplace-Young Excess Pressure Force Approximation

Another possibility for defining the force of pressure difference across a curved fluid surface, similar to Eq. 5, is the direct application of the Laplace-Young equation. Every point on the surface separating a liquid and gas has a maximum and a minimum radius of curvature, R_1 and R_2 , respectively. These occur in planes that are perpendicular to each other, and that are both perpendicular to the tangent plane of the surface. The Laplace-Young equation relates the excess pressure across the surface at any point to the principal radii of curvature at the point by

$$p = \gamma_s \left(\frac{1}{R_1} + \frac{1}{R_2} \right).$$

Employing similar ideas as in previous sections we can derive the second form of the force due to the excess pressure at particle i as

$$F_{laplaceyoung}^i = 2w_0 \gamma_s \left(\frac{1}{R_{1i}} + \frac{1}{R_{2i}} \right) A_i N_i. \quad (6)$$

For a spherical bubble the principal radii of curvature are equal to its radius, that is $R_{1i} = R_{2i} = r$ and mean curvature $H = 0.5(1/R_{1i} + 1/R_{2i}) = 1/r$. Therefore, the Equation 6 is the generalization of Equation 5. The first form of excess force, F_{excess} , is a good approximation for a spherical bubble, giving a smaller error than the second form, $F_{laplaceyoung}$, which uses two approximations of principal radii. Nevertheless, the last form is applicable to bubbles that have lost their spherical shapes, particularly when they are in collision or coalescence.

5.4. Drag Force

Bubbles immersed in moving fluid experience forces from shear stress and pressure differences caused by fluid motion.

In general, drag cannot be predicted analytically, and thus for most purposes it is calculated experimentally.

It can be shown ² that the force of a uniform flow with speed \mathbf{v} striking a flat surface of area A is resolved into normal and tangential components as

$$F_{drag}^n = \alpha_n A |\mathbf{v}| \mathbf{v}_r^n,$$

$$F_{drag}^t = \alpha_t A \mathbf{v}_r^t.$$

Assuming a surface with velocity \mathbf{v}_s , the relative velocity with respect to a fluid velocity \mathbf{v} is $\mathbf{v}_r = \mathbf{v} - \mathbf{v}_s$. The scaling constants α_n , and α_t depend on the viscosity of the surrounding field. The drag force is uniquely distributed among all particles forming the flat surface, usually formed by three particles of a triangular patch.

5.5. Bubble Coalescence

From the similar behavior observed in bubbles in a cluster and in atomic arrangements in a lattice, it is found that when the centers of two bubbles having the same size are separated by a distance that is large compared with the diameter of the bubbles, the force of attraction is very weak. As the separation between bubbles decreases, the force of attraction increases. This force reaches a maximum when the bubbles just come into contact. When the separation is decreased further the force of attraction rapidly decreases and becomes strongly repulsive. The repulsive nature of the force is due to the fixed amount of air in each bubble. The area, A_c , of the common surface separating the bubbles slowly increases and consequently the repulsive force increases. The repulsive force F_{rep}^A pointing from the first bubble center is

$$F_{rep}^A = p_A A_c,$$

where p_A is the internal pressure of the bubble.

5.6. Energies of Interaction between Film Surfaces

Interbubble interactions can be described by Lennard-Jones' potential energy, often used by physicists in molecular dynamics simulations and expressed as:

$$E_{lennard} = \left(\frac{d}{|r|}\right)^{2n} - 2\left(\frac{d}{|r|}\right)^n,$$

where the threshold d represents the zone of minimum potential, n is a parameter and $|r| = |B - A|$ is the length of the vector connecting two bubble centers. The force derived from this potential is

$$F_{lennard} = -\frac{\partial E_{lennard}}{\partial B} = 2n \frac{d^n}{|r|^{n+2}} \left(\frac{d^n}{|r|^n} - 1\right) \frac{r}{|r|}. \quad (7)$$

Figure 8 sketches the graph of energy potential, $E_{lennard}$, and the magnitude of corresponding repulsive force $|F_{lennard}|$.

Assuming two bubbles of radii r_A and r_B , Plateau's laws

can be introduced to Eq. 7 from Eq. 2 by writing the resting distance

$$d = r_A^2 + r_B^2 - r_A r_B.$$

This force attracts the centers of the two bubbles until they reach the optimum distance d , thus creating a meeting angle of 120° between the bubbles.

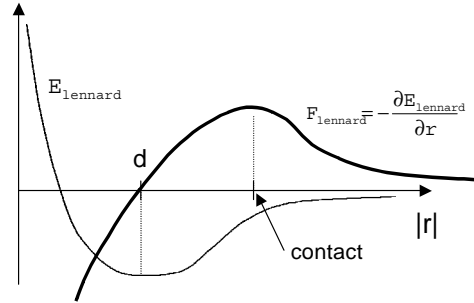


Figure 8: Coalescence of two bubbles: energy potential (thin line) and repulsive force (bold line).

5.7. Bubble Plane Interaction

The bubble with radius r_A will produce a hemisphere when it collides with a wet planar surface. The contact area of the bubble and the surface slowly increases and consequently the radius of the hemisphere, r_h , increases to a maximum, $r_h = \sqrt[3]{2} r_A$. The force from excess pressure, p_A , acting vertically upwards on the hemispherical section of bubble is known to be

$$p_A A_p,$$

where A_p is the contact area with the plane. Utilizing the above fact, the plane interaction force at each particle not in collision is proposed to be a fraction force in the direction of its normal vector N_i as follows

$$F_{plane}^i = w_i p_A A_p N_i, \quad \sum w_i = 1, \quad (8)$$

where w_i is the weighting parameter. The contact area can be calculated as the area of all triangular patches, of subdivided bubble, belonging to the plane. The effect of plane interaction force, F_{plane} , can be seen in Figure 9. Please, note the increase of the bubble radius. With this understanding of the bubble plane collision for a horizontal plane orientation, the question arises whether a hemispherical surface appears for all orientations of the plane? As the gravitational force is negligible compared with the surface tension force, the hemispherical shape is solely due to surface tension for the liquid-air interface. Particles in collision with the plane are influenced by additional force from surface tension for the liquid-solid interface. This force determines whether the bubble absorbed in to the solid surface, pops or forms a hemisphere. For simplicity, the planar surface is assumed to

be wet and thus the surface tension for the liquid-solid interface is zero. As a result, the hemispherical surface will slide down a non-horizontal planar surface.

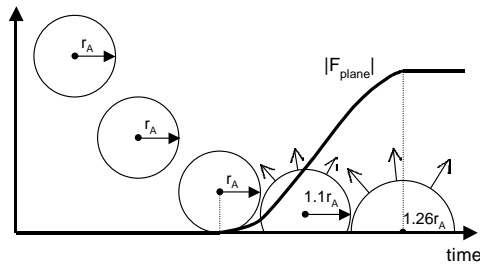


Figure 9: F_{plane} force is monotonically increasing in time from 0 to $p_A A_p$ during bubble collision with a plane.

6. Results

The proposed method has been implemented as our bubble simulator. Even though our models are fairly large, we are able to follow the progression of simulation interactively on our SGI O2 when the number of bubbles does not exceed six. A simulation preview can be visualized as a wire-frame or a simple Open GL model. When high-quality frames are required, the system can generate POV-Ray ray-tracing scene files automatically for animation purposes.

Before being able to create an adequate simulation, we had to establish spring parameters and scaling constants of external forces. Initially, the bubble position, its size and environment parameters such as wind flow forces are given as input. The system then determines the number of particles needed for surface approximation and the rest length of springs, and locates the bubble center. When a particle collides with the environment or the surface patch of the other bubble, only the tangent component of external force is used in calculating particle speed. We keep track of all bubbles in collision by storing them in a collision matrix. Once two bubbles are in collision they will remain forever in collision. Their speed will be calculated as the average of their respective centers, and coalescence forces are employed. In the current implementation the equation of motion is integrated by Euler's explicit method with time step $t = 0.02 s$. Development of an implicit integration method is currently underway.

Several successful simulations have been completely calculated and visualized. The first example demonstrates the spring force that enables the surface to simulate natural movement of an elastic object, representing the tension force that tends to minimize the surface, and on the other hand, the excess pressure force that tends to maintain convexity of the surface and increase the surface area. The total influence of such forces creates spherical bubbles as observed in

nature. Bubble motion and deformation by an external fluid are shown in the left of Figure 10.

The next simulation was performed to show the bubble colliding with a plane and to demonstrate the response to F_{plane}^i force shown in Figure 10 right.

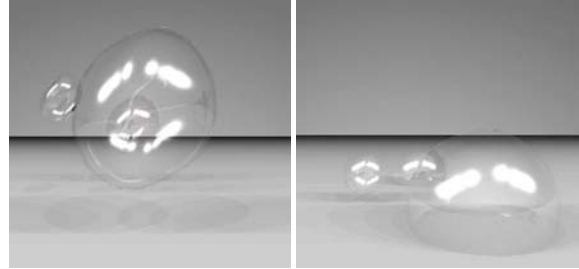


Figure 10: Deformation of bubble and bubble after collision with plane.

Another interesting process successfully simulated is the creation of a bubble from a tube. Initially, the particles at the end of the tube form the disk with boundary particles nailed to the tube by constraints. Particles are connected by springs with short rest lengths. Next, constant air flow through the tube starts deforming the shape. During the creation process the rest length of spring is monotonically increased to a maximum limit. The limit is derived based on the predefined size of bubble just created. Finally, when the bubble grows to its maximum size, the hole at the end of tube is closed with additional triangular patches. For simplicity, the hole is formed by four particles arranged in a square. The screen shots of a bubble creation generated with the proposed simulator are shown in the top row of Figure 11, while the bottom row shows the composition of those simulated shapes with an animated scene.

The third example, shown in Figure 12, simulates bubble coalescence between two bubbles, employing both the repulsive force F_{rep}^A and surface-interaction force F_{lenard} . Those forces are acting on the bubble center that can be difficult to determine in bigger clusters.

Particles forming the interface surfaces, after the coalescence of the two bubbles, moved freely without any constraints in our simulations. One reason for this unnatural movement may be the large rest length of springs forming the interface surface, which is actually equal to that of the original bubbles. This disturbing effect during the animation was eliminated by clipping out the interface surface and substituting it with a spherical cap that had proper curvature. Clipping was done directly in the ray-tracing program with set theoretic operations. It is not yet understood how to find the interface surface dynamically. However, Plateau's laws were successfully enforced between the outer bubble shells in our simulations.

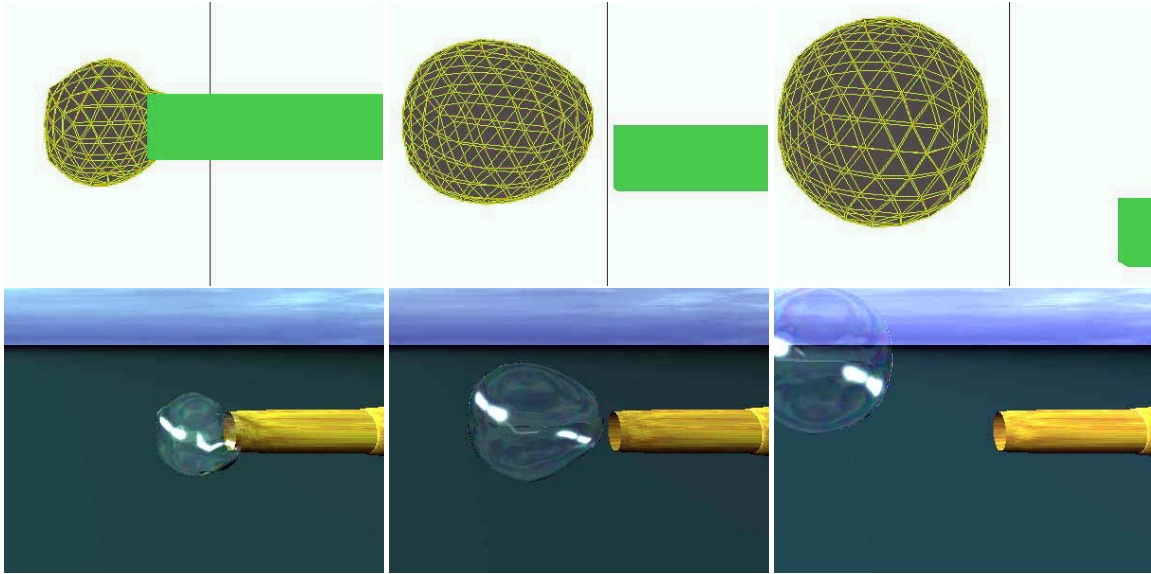


Figure 11: Bubble creation.



Figure 12: Forming double bubble.

Finally, Figure 13* shows a frame from an animation of a Japanese garden in which bubbles emerge from a bamboo fountain.

7. Conclusions

We have described a new model, which can be used for soap-bubble simulation and bubble-animation control, based on the Laplace-Young equation, Plateau's laws, and aerodynamics. In practice, application of the proposed methods is quite simple. Yet the new model allows us to simulate complex phenomena such as bubble creation, collision with a plane, and collision of multiple bubbles.

Certain mechanisms remain open problems for future investigation and implementation, including convection, evaporation and suction produced by pressure gradients, which cause water to drain from bubble film and thus thin the film.

Acknowledgements

The author wishes to thank Mr. Atsushi Umaki and Takuo Kadoya for their help in generating the animation frames and pictures for this paper. The images were rendered by the POV-Ray ray-tracing program developed by POV-Team. This research was sponsored by grants from the Fukushima Prefectural Foundation in Japan for the Advancement of Science and Education.



Figure 13: *Bubble fountain in Japanese garden.*